

Investigating Electronic Coherences in Conjugated Polymers via Two-Dimensional Electronic Coherence Spectroscopy

William Barford,^{1, 2, a)} Allison Nicole Arber,^{1, 2} and Fynn McLennan^{1, 3}

¹⁾*Department of Chemistry, Physical and Theoretical Chemistry Laboratory, University of Oxford, Oxford, OX1 3QZ, United Kingdom*

²⁾*Balliol College, University of Oxford, Oxford, OX1 3BJ, United Kingdom*

³⁾*Magdalen College, University of Oxford, Oxford, OX1 4AU, United Kingdom*

We propose a two-dimensional electronic coherence spectroscopy protocol for determining the time-dependent coherences between the stationary states of a system induced by a time-dependent system-bath interaction. We also investigate the role of temporally-correlated noise on coherence dephasing. This protocol enables dynamical information about the system and its coupling to the environment to be determined. We show how this protocol can be used to investigate exciton dynamics in conjugated polymers induced by the coupling of their torsional modes with the environment.

^{a)}Electronic mail: william.barford@chem.ox.ac.uk

I. INTRODUCTION

The question of whether electronic coherences exist in optically excited macromolecular systems, e.g., π -conjugated polymers and light harvesting complexes, has been an outstanding one for a number of years^{1–6}. This question is motivated by the attempt to understand how coherences — if they exist — can survive under ambient conditions. It is also motivated by the expectation that coherences might⁷ enhance the efficiency of energy and charge transport, thus improving the efficiency and providing design principles for synthetic photovoltaic devices.

Recently, borrowing concepts from quantum information theory, quantum process tomography has been proposed as a method to ‘witness’ electronic coherences^{8–10}. In this paper we propose a conceptually straightforward protocol based on the well-established technique of two-dimensional electronic coherence spectroscopy (2D-ECS) to determine dynamical coherences.

Before discussing how coherences are established and measured, let us first define what we mean by them. In this paper we define electronic coherences as the off-diagonal matrix elements of the system’s density matrix when expressed in the energy eigenbasis of the system. Such coherences in a system can be induced via coupling to the environment in a variety of ways. For example, a coherent light source might excite a number of energy eigenstates, thus creating a non-stationary state. In this case, assuming no dephasing or dissipation, the populations are constant, while coherences have constant magnitudes but oscillate with the transition angular frequencies. A more interesting scenario is when the excited system interacts with an environment that couples these eigenstates and hence causes interstate transitions. This will cause population transfers and the magnitude of the coherences will change in time. Moreover, if the energy eigenstates are spatially separated, it will cause energy transfer. It is this latter scenario that we investigate in this paper.

Here, we set up a simple two-level system subject to a time-dependent periodic perturbation. We show how the induced coherences can be observed via a particular 2D-ECS protocol. This results in a characteristic fingerprint of dynamical coherences, from which dynamical information about the system and environment can be determined. We then investigate how a noisy (dephasing) environment destroys the coherences.

Having established this model system, we next discuss how it might be realized in practice.

In particular, we envisage a conjugated polymer subject to torsional fluctuations via the Brownian impulses of its environment. We derive realistic parameters for both intra and inter chromophore energy transfer, and investigate whether the coherence signals described in Section III might be observed in practice.

II. TWO-LEVEL SYSTEM

A. Model

The excited-state Hilbert space of our two-level system is spanned by the energy eigenkets $|a\rangle$ and $|b\rangle$ with energies E_a and E_b . Thus, the system Hamiltonian is

$$\hat{H}_S = E_a |a\rangle \langle a| + E_b |b\rangle \langle b| \quad (1)$$

and for convenience we define the Rabi angular frequency $\omega_0 = (E_b - E_a)/\hbar > 0$.

The system is coupled to a bath via the perturbation

$$\hat{H}_{SB} = V(t) (|a\rangle \langle b| + |b\rangle \langle a|), \quad (2)$$

where we take the system-bath interaction, $V(t)$, to be of the general form

$$V(t) = 2\epsilon \cos(\omega t + \phi(t)). \quad (3)$$

Here, $\phi(t)$ acts as a temporally-correlated phase that causes dephasing of the coherences. In particular, as described in Section III B, we will choose $\phi(t)$ so that the autocorrelation function of the system-bath interaction satisfies

$$\langle V(t)V(0) \rangle = |V(0)|^2 \cos(\omega t) \exp(-\gamma t), \quad (4)$$

where γ is the dephasing rate.

B. Preparation of the Initial State

Under the influence of a sufficiently narrow electric field pulse centered at $t = 0$, i.e., $\underline{E}(t) = \underline{\alpha}\varepsilon(t)$, where $\underline{\alpha}$ is the polarization and $\varepsilon(t)$ is the intensity, the initial excited state vector is^{11,12}

$$|\Psi(t=0)\rangle = \frac{i}{\hbar} \sum_{i=a}^b \underline{\alpha} \cdot \underline{\mu}_j \tilde{\varepsilon}(\omega_j) |i\rangle. \quad (5)$$

Here, $\underline{\mu}_j = \langle j | \underline{\mu} | GS \rangle$ is the transition dipole moment and $\tilde{\varepsilon}(\omega_j)$ is the Fourier transform of $\varepsilon(t)$ evaluated at the transition angular frequency $\omega_j = E_j/\hbar$. We see that both $\underline{\alpha} \cdot \underline{\mu}_j$ and $\tilde{\varepsilon}$ determine the amplitudes of the eigenkets in $|\Psi(t=0)\rangle$; we return to this observation in Section IV.

C. Solution of the Time-Dependent Schrödinger Equation

The general time-dependent state vector for the two-level system is

$$|\Psi(t)\rangle = \psi_a(t) \exp(-iE_a t/\hbar) |a\rangle + \psi_b(t) \exp(-iE_b t/\hbar) |b\rangle. \quad (6)$$

The dynamics of this system can be experimentally determined via 2D-ECS using the protocol described in the next section, for which the initial conditions are $\psi_a(0) = 0$ and $\psi_b(0) = 1$. Then, employing the rotating-wave or secular approximation (RWA)¹³, for a time-dependent perturbation given by

$$V(t) = 2\epsilon \cos(\omega t + \chi), \quad (7)$$

with a time-independent phase χ , we obtain

$$\psi_a(t) = \left(\frac{\epsilon}{\hbar\alpha} \right) \exp(i\chi) \exp(i\Delta\omega t/2) (\exp(i\alpha t/2) - \exp(-i\alpha t/2)) \quad (8)$$

and

$$\psi_b(t) = \frac{1}{2} \exp(-i\Delta\omega t/2) \left(\left(1 + \left(\frac{\Delta\omega}{\alpha} \right) \right) \exp(i\alpha t/2) + \left(1 - \left(\frac{\Delta\omega}{\alpha} \right) \right) \exp(-i\alpha t/2) \right). \quad (9)$$

The off-resonance parameter is

$$\Delta\omega = (\omega - \omega_0) \quad (10)$$

and we define

$$\alpha = ((\Delta\omega)^2 + (2\epsilon/\hbar)^2)^{1/2}. \quad (11)$$

The time-dependent system-bath interaction causes population to be exchanged between $|b\rangle$ and $|a\rangle$ with a time period $T_\epsilon = 2\pi/\alpha$. For the pure quantum state defined by Eq. (6) the populations of the eigenkets are $|\psi_a(t)|^2$ and $|\psi_b(t)|^2$, while their coherences are $\psi_a^*(t)\psi_b(t)$. Off-resonance (i.e., $\Delta\omega \neq 0$) there is an incomplete transfer of population with the maximum population of $|a\rangle$ being $4(\epsilon/\hbar\alpha)^2$.

We notice the phase factor of $\exp(i\chi)$ in the expression for $\psi_a(t)$, which arises from the $t = 0$ phase in $V(t)$. As explained in Section III, this phase factor has important implications for the definition of $|\Psi_\delta\rangle$, which is created at a time t_1 after $|\Psi_\alpha\rangle$ at which point $\chi = \omega t_1$.

III. TWO DIMENSIONAL SPECTROSCOPY

Using quantum trajectories, we can compute the two-dimensional electronic coherence spectrum using the method described by Marcus *et al.*¹⁴. In the following we compute one of the rephasing diagrams, labeled ‘B’ in ref¹⁴ and R_1 in ref¹⁵.

Denoting the creation operators for the eigenkets $|a\rangle$ and $|b\rangle$ as \hat{a}_a^\dagger and \hat{a}_b^\dagger , respectively, we define the first-order trajectory as

$$|\Psi_\delta\rangle = \hat{U}(t_\gamma, t_\delta)\hat{O}_\delta|\text{GS}\rangle, \quad (12)$$

where $\hat{O}_\delta = \hat{a}_b^\dagger$ and $\hat{U}(t_\gamma, t_\delta)$ is the evolution operator determined by \hat{H}_S and \hat{H}_{SB} . Thus, $|\Psi_\delta\rangle$ is an excitation from the groundstate to $|b\rangle$ at time t_δ , followed by evolution in the excited state manifold (ESM) under the action of $(\hat{H}_S + \hat{H}_{SB})$ to time t_γ , by which time it has acquired amplitude in both $|a\rangle$ and $|b\rangle$. This trajectory is illustrated schematically in red in Fig. 1.

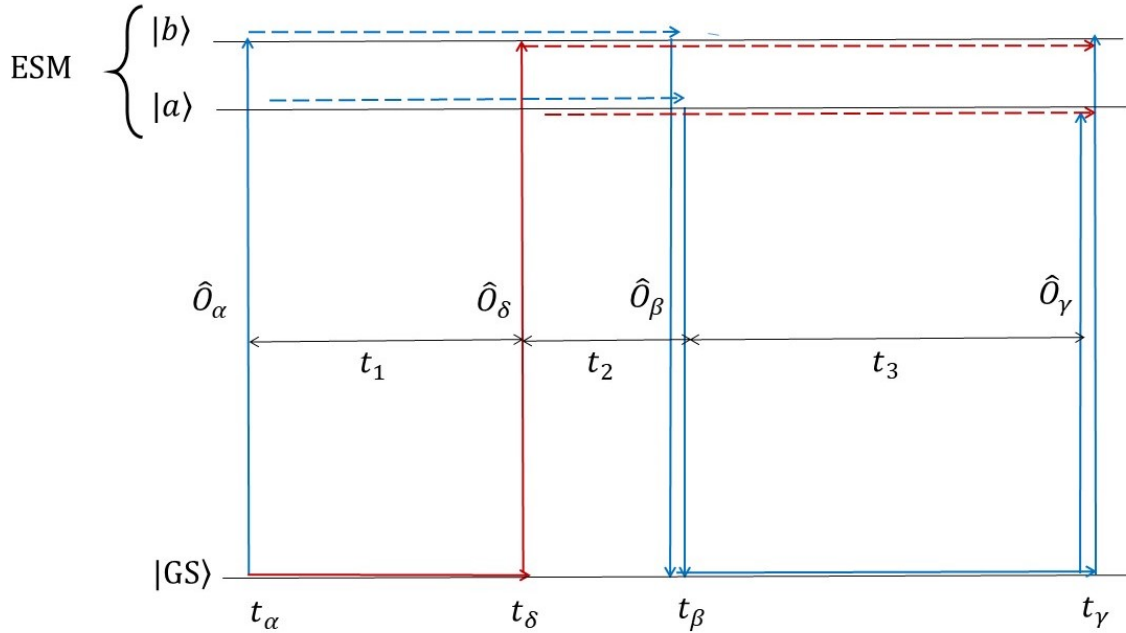


FIG. 1. A diagram illustrating the evolution of the first-order trajectory, $|\Psi_\delta\rangle$, (in red) and the third-order trajectory, $|\Psi_{\alpha\beta\gamma}\rangle$, (in blue). The overlap $\langle\Psi_{\alpha\beta\gamma}|\Psi_\delta\rangle$ corresponds to the rephasing diagram labeled ‘B’ in ref¹⁴ and R_1 in ref¹⁵.

Similarly, we define the third-order trajectory as

$$|\Psi_{\alpha\beta\gamma}\rangle = \hat{O}_\gamma \hat{U}(t_\gamma, t_\beta) \hat{O}_\beta \hat{U}(t_\beta, t_\alpha) \hat{O}_\alpha |\text{GS}\rangle, \quad (13)$$

where $\hat{O}_\alpha = \hat{a}_b^\dagger$, $\hat{O}_\beta = (\hat{a}_a + \hat{a}_b)/\sqrt{2}$ and $\hat{O}_\gamma = (\hat{a}_a^\dagger + \hat{a}_b^\dagger)/\sqrt{2}$. Thus, $|\Psi_{\alpha\beta\gamma}\rangle$ is an excitation from the groundstate to $|b\rangle$ at time t_α , evolution in the ESM under the action of $(\hat{H}_S + \hat{H}_{SB})$ to time t_β , de-excitation via a linear combination of $|a\rangle$ and $|b\rangle$ to the groundstate at time t_β , evolution in the groundstate to time t_γ , and finally excitation via a linear combination of $|a\rangle$ and $|b\rangle$ at time t_γ . This trajectory is illustrated schematically in blue in Fig. 1.

By a time t_β the state $|\Psi_\alpha\rangle = \hat{U}(t_\beta, t_\alpha) \hat{O}_\alpha |\text{GS}\rangle$ has acquired amplitude in both $|a\rangle$ and $|b\rangle$. These amplitudes are transferred to the groundstate via \hat{O}_β and re-excited at t_γ via \hat{O}_γ . The interference of these amplitudes with those of $|\Psi_\delta\rangle$, via the overlap $\langle \Psi_{\alpha\beta\gamma} | \Psi_\delta \rangle$, allow the dynamics — and in particular, the coherences — of the system to be determined.

Defining the time variables as $t_1 = t_\delta - t_\alpha$ (coherence time), $t_2 = t_\beta - t_\delta$ (waiting time) and $t_3 = t_\gamma - t_\beta$ (echo time), and Fourier transforming with respect to t_1 and t_3 , we obtain the two-dimensional in frequency-space and one-dimensional in time-space third-order response,

$$C_B(\omega_1, t_2, \omega_3) = \int \langle \Psi_{\alpha\beta\gamma} | \Psi_\delta \rangle \exp(i(\omega_1 t_1 + \omega_3 t_3)) dt_1 dt_3. \quad (14)$$

A. Analytical Results

Since the wavefunction overlap, $\langle \Psi_{\alpha\beta\gamma} | \Psi_\delta \rangle$, obtained via the RWA (i.e., Eq. (8) and (9)) is a sum of a product of complex exponentials, its Fourier transform with respect to t_1 and t_3 results in a sum of a product of delta-functions. In particular, $C_B(\omega_1, t_2, \omega_3)$ corresponds to four sets of four-peaks. Referring to Fig. (2), we identify the four sets as follows.

- The set A are associated with the population of $|b\rangle$:

$$\begin{aligned} & \frac{1}{4} \left(1 \mp \frac{\Delta\omega}{\alpha} \right)^2 \delta(\omega_1 + (\omega_b + (\Delta\omega \pm \alpha)/2)) \delta(\omega_3 - (\omega_b + (\Delta\omega \pm \alpha)/2)) \\ & + \frac{1}{4} \left(1 - \left(\frac{\Delta\omega}{\alpha} \right)^2 \right) \delta(\omega_1 + (\omega_b + (\Delta\omega \pm \alpha)/2)) \delta(\omega_3 - (\omega_b + (\Delta\omega \mp \alpha)/2)) \exp(\pm i\alpha t_2), \end{aligned} \quad (15)$$

where α is given by Eq. (11).

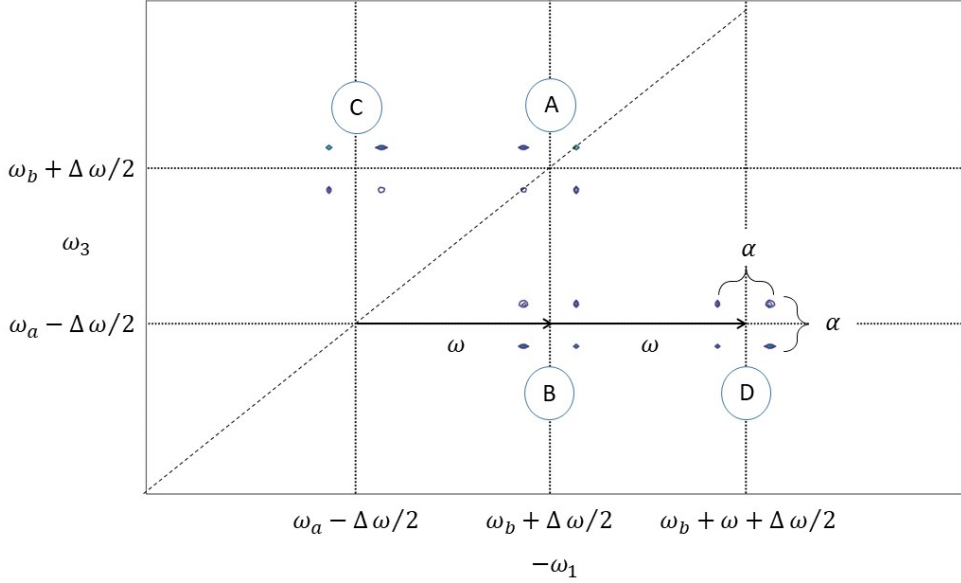


FIG. 2. The 2D-ECS spectrum for $\Delta\omega/\omega = 0.9$ and $\epsilon/\hbar\omega_0 = 0.25$. These results are obtained by computing the overlap $\langle \Psi_{\alpha\beta\gamma} | \Psi_\delta \rangle$ numerically using the TNT Library¹⁶ (as described in Section III B) and evaluating Eq. (14) using a discrete Fourier transform. The positions of the peaks correspond to Eq. (15) - (18). $\Delta\omega = \omega - \omega_0$ and α is defined in Eq. (11).

- The set B are associated with the population of $|a\rangle$:

$$\begin{aligned} & \left(\frac{\epsilon}{\hbar\alpha}\right)^2 [\delta(\omega_1 + (\omega_a + \omega - (\Delta\omega \pm \alpha)/2))\delta(\omega_3 - (\omega_a - (\Delta\omega \pm \alpha)/2)) \\ & - \delta(\omega_1 + (\omega_a + \omega - (\Delta\omega \pm \alpha)/2))\delta(\omega_3 - (\omega_a - (\Delta\omega \mp \alpha)/2)) \exp(\pm i\alpha t_2)]. \end{aligned} \quad (16)$$

- The set C are associated with coherences between $|a\rangle$ and $|b\rangle$:

$$\begin{aligned} & \mp \frac{\epsilon}{2\hbar\alpha} \left(1 \mp \frac{\Delta\omega}{\alpha}\right) \delta(\omega_1 + (\omega_a - (\Delta\omega \mp \alpha)/2))\delta(\omega_3 - (\omega_b + (\Delta\omega \pm \alpha)/2)) \exp(-i\omega t_2) \\ & \mp \frac{\epsilon}{2\hbar\alpha} \left(1 + \frac{\Delta\omega}{\alpha}\right) \delta(\omega_1 + (\omega_a - (\Delta\omega \pm \alpha)/2))\delta(\omega_3 - (\omega_b + (\Delta\omega \mp \alpha)/2)) \exp(-i(\omega \mp \alpha)t_2). \end{aligned} \quad (17)$$

- Similarly, the set D are associated with coherences between $|a\rangle$ and $|b\rangle$:

$$\begin{aligned}
& \mp \frac{\epsilon}{2\hbar\alpha} \left(1 \mp \frac{\Delta\omega}{\alpha} \right) \delta(\omega_1 + (\omega_b + \omega - (\Delta\omega \pm \alpha)/2)) \delta(\omega_3 - (\omega_a + (\Delta\omega \pm \alpha)/2)) \exp(i\omega t_2) \\
& \mp \frac{\epsilon}{2\hbar\alpha} \left(1 + \frac{\Delta\omega}{\alpha} \right) \delta(\omega_1 + (\omega_b + \omega + (\Delta\omega \pm \alpha)/2)) \delta(\omega_3 - (\omega_a - (\Delta\omega \mp \alpha)/2)) \exp(i(\omega \mp \alpha)t_2).
\end{aligned} \tag{18}$$

From these results we make the following general observations:

1. In the absence of induced coherences, i.e., when $V(t) = 0$, the system would remain in the stationary state $|b\rangle$ and there would be a single population peak at $(-\omega_b, \omega_b)$.
2. With induced coherences, however, there are four sets of four peaks. These sets of peaks correspond to the populations of $|b\rangle$ (i.e., at A) and $|a\rangle$ (i.e., at B), and their coherences (i.e., C and D).
3. Notice, however, that the two sets of peaks at $\omega_3 = \omega_a - \Delta\omega/2$ (i.e., B and D) are displaced along the $-\omega_1$ axis by ω . This ‘boost’ along ω_1 at $\omega_3 = \omega_a - \Delta\omega/2$ is a consequence of the phase factor $\chi = \omega t_1$ that the amplitude of $|a\rangle$ acquires when $|\Psi_\delta\rangle$ is created, as shown by Eq. (8).
4. Each set of peaks is split into four peaks whose splitting is determined by $\alpha = 2\pi/T_\epsilon$, where T_ϵ is the population transfer period.
5. Items (3) and (4) illustrate the characteristic 2D-spectrum obtained via this 2D-ECS protocol that provides a characteristic fingerprint of induced dynamical coherences.
6. The peaks exhibit complex dynamics as a function of t_2 . For example, the off-diagonal components of the population set of peaks oscillate with a period of T_ϵ , while the diagonal components of the coherence set of peaks oscillate with a period of $T = 2\pi/\omega$.
7. The intensity of the coherence peaks (i.e., C and D) relative to the dominant population peak (i.e., A) is proportional to $2\epsilon/\hbar\alpha$, and is a measure of the strength of the coherences. Similarly, the intensity of the population peak B relative to A is proportional to $(2\epsilon/\hbar\alpha)^2$, and is a measure of the maximum population transfer between $|b\rangle$ and $|a\rangle$.

8. All but one of the peaks in set A vanish for off-resonance if $2\epsilon \ll \hbar\alpha$, as in this case no coherences between $|b\rangle$ and $|a\rangle$ are established.

B. Dephasing

To mimic a noisy environment, we assume that the system-bath interaction satisfies the autocorrelation function defined by Eq. (4). As we discuss in the next section, this represents the autocorrelation function of monomer rotations caused by the Brownian fluctuations of the environment. Thus, the phase in Eq. (3) is

$$\phi(t) = \int_0^t \delta\omega(t')dt', \quad (19)$$

where $\delta\omega(t)$ is a temporally-correlated noise whose autocorrelation function satisfies

$$\langle \delta\omega(t)\delta\omega(0) \rangle = \delta\omega^2 \exp(-t/\tau_c). \quad (20)$$

To achieve Eq. (4) we require the ‘homogeneous’ limit, i.e., $\delta\omega\tau_c \ll 1$ ^{15,17}.

The numerical solutions of the time-dependent Schrödinger equation with a stochastic perturbation defined by Eq. (3) and Eq. (19) are performed via a Trotter decomposition of the evolution operator using the TNT Library¹⁶. By performing an ensemble average over 100 quantum trajectories with different temporal disorder we construct the system’s reduced density matrix.

The effect of a system-bath dephasing interaction is illustrated in Fig. 3. Fig. 3(a) shows that the populations of $|a\rangle$ and $|b\rangle$ equilibrate over time with a relaxation time $T_1 = \gamma^{-1}$, while Fig. 3(b) shows that the coherences between $|a\rangle$ and $|b\rangle$ decay in time with a dephasing time $T_2 = 2T_1$.

The effect of dephasing on the 2D-ECS spectrum is shown in Fig. 4. For fast dephasing ($\gamma^{-1} = T_\epsilon/4$, where T_ϵ is the population transfer period), coherences between $|a\rangle$ and $|b\rangle$ do not have time to become fully established, so a single population peak A dominates the spectrum. For intermediate dephasing ($\gamma^{-1} = T_\epsilon$), however, coherences are established, but noise destroys the resolution of each of the four sub-peaks within a set of peaks. Nevertheless, one of the characteristic fingerprints of induced dynamical coherences, namely the boost along ω_1 at $\omega_3 = \omega_a - \Delta\omega/2$, is still evident.

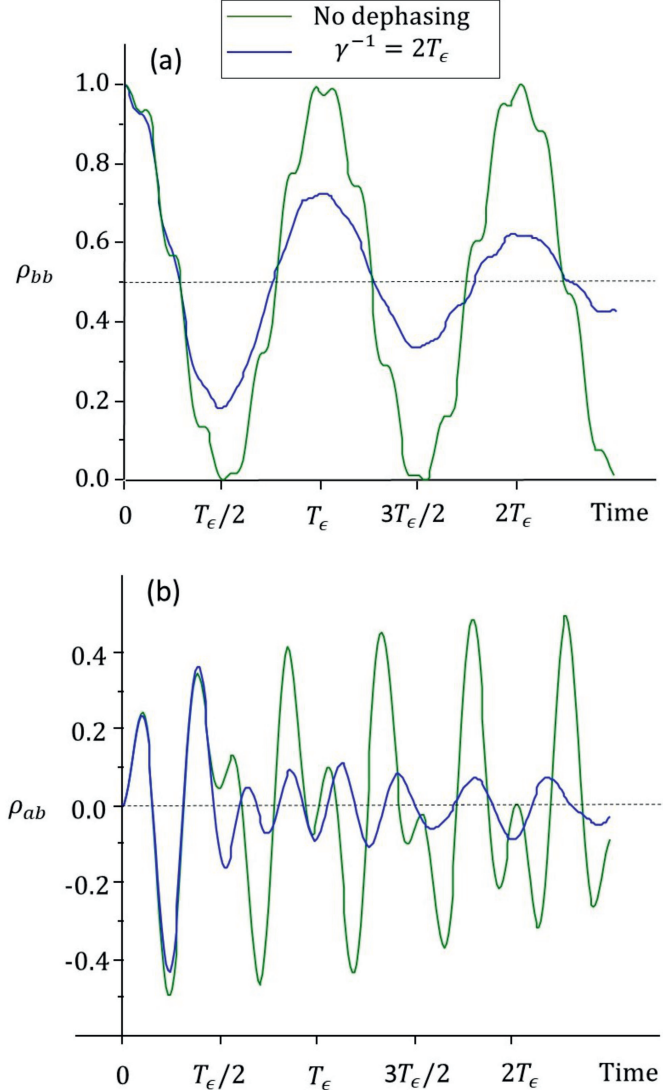


FIG. 3. (a) The population of $|b\rangle$, ρ_{bb} , as a function of time at resonance, $\omega = \omega_0$ (where $\rho_{aa} = 1 - \rho_{bb}$). (b) The coherences between $|a\rangle$ and $|b\rangle$, ρ_{ab} , as a function of time. The autocorrelation function of the system-bath interaction satisfies Eq. (4). Green (no dephasing), blue (dephasing time $\gamma^{-1} = 2T_\epsilon$, where T_ϵ is the population transfer period). Note that in the case of no-dephasing $\rho_{bb}(t)$ deviates from $|\psi_b(t)|^2$ with $\psi_b(t)$ given by Eq. (9) because this is a numerically exact solution of the two-level system and not the RWA.

IV. REALISTIC MODEL

So far we have considered a theoretical two-level system and have shown how the dynamics of that system can be observed via 2D-ECS. In this section we describe practical realizations

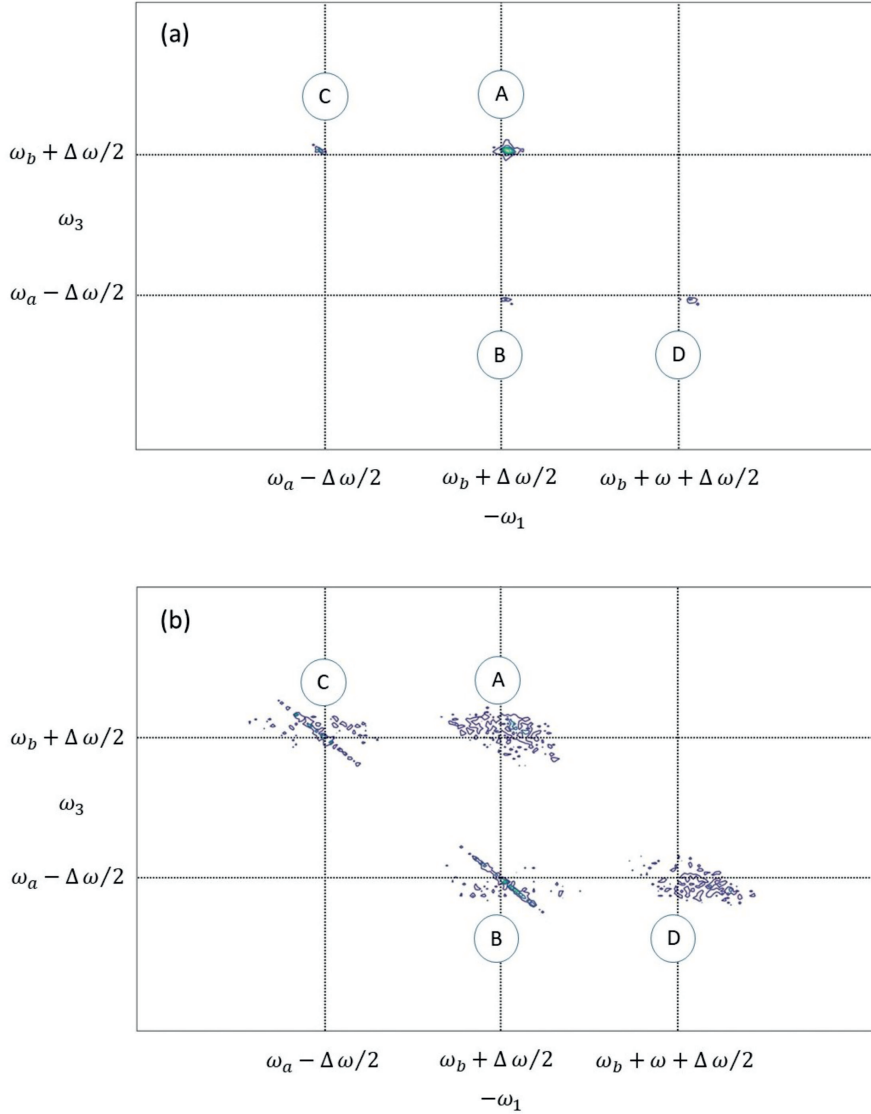


FIG. 4. The effect of dephasing on the 2D-ECS spectrum. (a) fast dephasing: $\gamma^{-1} = T_\epsilon/4$ and (b) intermediate dephasing: $\gamma^{-1} = T_\epsilon$, where $T_\epsilon = 2\pi/\alpha$ is the population transfer period. $\Delta\omega/\omega = 0.9$ and $\epsilon/\hbar\omega_0 = 0.25$.

of that system. In particular, we consider two examples of exciton dynamics in conjugated polymer systems. Before describing these examples in detail, we first review the mapping of a model of excitons to the two-level system.

A. The Frenkel Exciton Model

The dynamics of Frenkel excitons in conjugated polymers is described by the Frenkel exciton model¹⁸, defined by

$$\hat{H} = \sum_{n=1}^N \epsilon_n |n\rangle \langle n| + \sum_{n=1}^{N-1} J_n(t) (|n\rangle \langle n+1| + |n+1\rangle \langle n|), \quad (21)$$

where n labels a monomer and ϵ_n is the excitation energy of a monomer. J_n is the exciton transfer integral,

$$J_n(t) = J_{DD} + J_{SE} \cos^2 \theta_n(t), \quad (22)$$

where J_{DD} is the through-space, dipole-dipole contribution, $J_{SE} \cos^2 \theta_n(t)$ is the through-bond, superexchange contribution, and θ_n is the dihedral angle between monomers. In general, $\theta_n(t) = \theta + \delta\theta_n(t)$, where the dynamical component $\delta\theta_n(t)$ arises from thermal fluctuations.

Assuming that $\delta\theta_n(t) \ll \theta$ we can linearize Eq. (22) to obtain

$$J_n(t) = J - J_{SE} \delta\theta_n(t) \sin 2\theta, \quad (23)$$

where

$$J = J_{DD} + J_{SE} \cos^2 \theta. \quad (24)$$

Thus, the system Hamiltonian is

$$\hat{H}_S = \sum_{n=1}^N \epsilon_n |n\rangle \langle n| + \sum_{n=1}^{N-1} J (|n\rangle \langle n+1| + |n+1\rangle \langle n|) \quad (25)$$

and the system-bath Hamiltonian is

$$\hat{H}_{SB} = -J_{SE} \sin 2\theta \sum_{n=1}^{N-1} \delta\theta_n(t) (|n\rangle \langle n+1| + |n+1\rangle \langle n|). \quad (26)$$

Transforming into the eigenkets of \hat{H}_S , i.e.,

$$|j\rangle = \sum_{n=1}^N c_{nj} |n\rangle, \quad (27)$$

we have the system Hamiltonian

$$\hat{H}_S = \sum_{j=1}^N E_j |j\rangle \langle j|, \quad (28)$$

where¹⁹ $E_j = 2J \sum_n c_{n,i} c_{n+1,i}$. Similarly, the system-bath Hamiltonian is

$$\hat{H}_{SB} = \sum_{ij} V_{ij}(t) |i\rangle \langle j|, \quad (29)$$

where

$$V_{ij}(t) = -J_{SE} \sin 2\theta \sum_{n=1}^{N-1} \delta\theta_n(t) (c_{n,i} c_{n+1,j} + c_{n,j} c_{n+1,i}) \quad (30)$$

(and we have neglected a time-dependent diagonal term that does not cause interstate conversion).

For a polymer subject to stochastic thermal fluctuations, the dynamical component of the torsional angle satisfies

$$\delta\theta_n(t) = \delta\theta \cos(\omega t + \phi_n(t)), \quad (31)$$

where $\delta\theta = (k_B T / K_{\text{rot}})^{1/2}$, ω is the rotational angular frequency and K_{rot} is the rotational force constant.

The mapping to the two-level system of Section II A is completed by retaining only two states in Eq. (28) and (29), and by noting that

$$2\epsilon = -J_{SE} \delta\theta \sin 2\theta \sum_{n=1}^{N-1} (c_{n,a} c_{n+1,b} + c_{n,b} c_{n+1,a}). \quad (32)$$

The next two sections give specific examples.

B. Energy Transfer

We first consider energy transfer between two almost orthogonal chromophores on a bent portion of a conjugated polymer, as shown in Fig. 5(a). In practice, chromophores are defined by the spatial extent of local exciton ground states (LEGSSs), whose spatial extent is determined by Anderson localization of the exciton center-of-mass wavefunction¹⁸. The boundary between chromophores is determined by the spatial distribution of disorder and possible ‘conjugation breaks’. In all cases, the LEGSSs overlap at the boundaries, meaning that Eq. (32) does not vanish. To achieve the protocol described in Section III, exciton $|b\rangle$ is first excited, which means that $\hat{O}_\alpha \propto \hat{\mu}_b$ and $\hat{O}_\delta \propto \hat{\mu}_b$. The transfer of amplitude to exciton $|a\rangle$ is then determined by setting $\hat{O}_\beta \propto (\hat{\mu}_a + \hat{\mu}_b)/\sqrt{2}$ and $\hat{O}_\gamma \propto (\hat{\mu}_a + \hat{\mu}_b)/\sqrt{2}$.

For a typical conjugated polymer at room temperature, e.g., poly(p-phenylene), $\delta\theta \approx 0.1$ rads, $J \approx 2$ eV and $J_{SE} \sin 2\theta \approx 1$ eV. The wavefunction overlap, $\sum_n (c_{n,a} c_{n+1,b} + c_{n,b} c_{n+1,a})$,

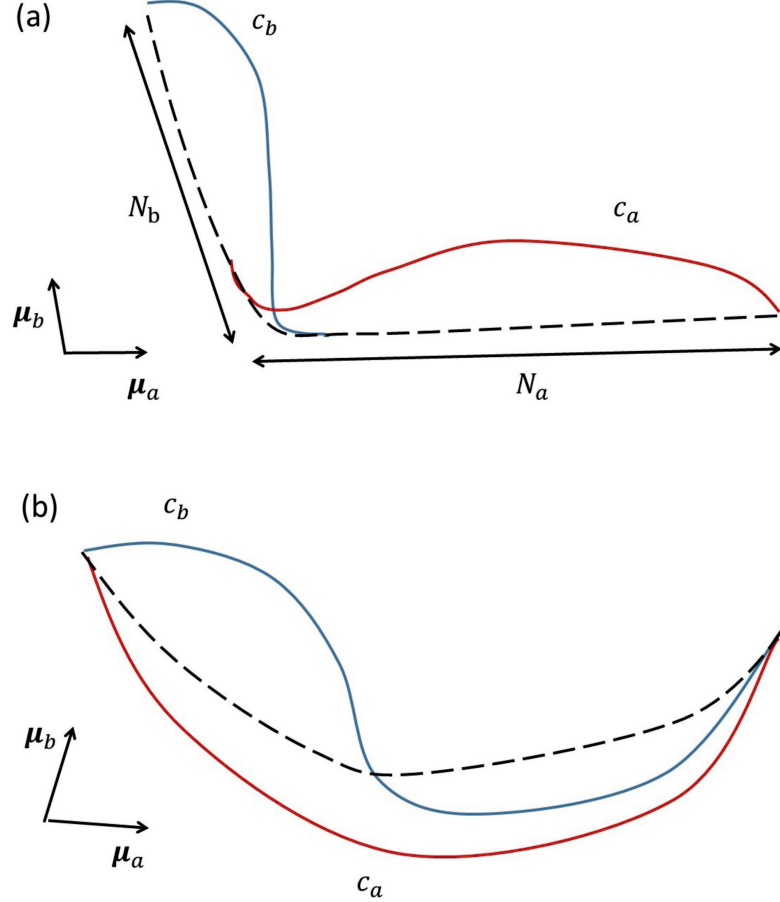


FIG. 5. (a) A schematic of the exciton center-of-mass wavefunctions c_a (in red) and c_b (in blue) on neighboring chromophores of a polymer segment (represented by the dashed black curve), where $N_b < N_a$. (b) A schematic of the exciton center-of-mass wavefunctions c_a (nodeless, shown in red) and c_b (with one node, shown in blue) on the same curved chromophore (represented by the dashed black curve). $\underline{\mu}_a$ and $\underline{\mu}_b$ represent the transition dipole moments of these states.

is determined by disorder, but is typically ~ 0.1 . Thus, $\epsilon \lesssim 0.005$ eV, implying at resonance a population transfer period $T_\epsilon \sim 1$ ps. The torsion oscillation energy is $\hbar\omega = 0.02$ eV and thus resonance is achieved if the difference in chromophore sizes satisfies $\Delta N/N^3 \approx 5 \times 10^{-4}$, e.g., $N_b = 18$ and $N_a = 22$. In this case $\epsilon/\hbar\omega_0 = 0.25$ which corresponds to the parameters for Fig. 2.

C. Energy Relaxation

As a second example we consider energy relaxation from a higher to a lower energy exciton, as shown in Fig. 5(b). Here, c_a is the LEGS while c_b is a locally excited exciton state (LEES)¹⁸. Importantly, c_b has one node so that on a curved chromophore its (non-zero) transition dipole moment is almost orthogonal to that of c_a ²⁰. To achieve the protocol described in Section III, $\hat{O}_\alpha \propto \hat{\mu}_b$, $\hat{O}_\delta \propto \hat{\mu}_b$, $\hat{O}_\beta \propto (\hat{\mu}_a + \hat{\mu}_b)/\sqrt{2}$ and $\hat{O}_\gamma \propto (\hat{\mu}_a + \hat{\mu}_b)/\sqrt{2}$. In this case, resonance is achieved if the chromophore size $N \approx 50$, when again $\epsilon/\hbar\omega_0 = 0.25$.

V. DISCUSSION AND CONCLUDING REMARKS

We have proposed a protocol for performing 2D-ECS experiments that determine induced time-dependent coherences between the stationary states of a two-level system. This protocol gives a rich 2D-ECS spectrum characteristic of dynamical coherences that differs from the observed coherences of the non-stationary state $|\Psi(t=0)\rangle = (|a\rangle + |b\rangle)/\sqrt{2}$. The 2D-ECS spectrum for the non-stationary state consists of populations at $(-\omega_a, \omega_a)$ and $(-\omega_b, \omega_b)$, and coherences at $(-\omega_a, \omega_b)$ and $(-\omega_b, \omega_a)$. In contrast, the 2D-ECS spectrum for induced dynamical coherences differs in two distinct ways. First, each peak splits into a set of four peaks, with the splitting of the peaks determined by the population transfer period, T_ϵ . Second, at $\omega_3 \sim \omega_a$ there is a boost along the ω_1 axis by ω , the angular frequency of the system-bath interaction that induces these dynamics. These two features imply that this proposed protocol provides a unique fingerprint for induced dynamical coherences and the system-bath interactions. However, for weak system-bath interactions coherences are only established at or close to resonance, i.e., $\omega \simeq \omega_0$. Furthermore, coherences are destroyed by strong dephasing, meaning that only the population at $(-\omega_b, \omega_b)$ would be observed.

We next discussed realistic exemplars of this model, namely a conjugated polymer whose torsional fluctuations act as the time-dependent perturbation. The two stationary states are either excitons localized on neighboring chromophores, or the two lowest excited states on the same chromophore. Since both the angular frequency of the torsional oscillations and the strength of the perturbation that drives the dynamics is small (i.e., $\sim 0.01 - 0.02$ eV) it is important that the system is on or close to resonance for coherences to be induced and observed via 2D-ECS.

DATA AVAILABILITY

The data that support the findings of this study are available from the corresponding author upon reasonable request.

REFERENCES

¹G. S. Engel, T. R. Calhoun, E. L. Read, T. K. Ahn, T. Mancal, Y. C. Cheng, R. E. Blankenship, and G. R. Fleming, *Nature* **446**, 782 (2007).

²A. Ishizaki and G. R. Fleming, *Proceedings of the National Academy of Sciences of the United States of America* **106**, 17255 (2009).

³I. Hwang and G. D. Scholes, *Chemistry of Materials* **23**, 610 (2011).

⁴G. D. Scholes, G. R. Fleming, A. Olaya-Castro, and R. van Grondelle, *Nature Chemistry* **3**, 763 (2011).

⁵A. Chenu and G. D. Scholes, *Annual Review of Physical Chemistry* **66**, 69 (2015).

⁶J. C. Dean and G. D. Scholes, *Accounts of Chemical Research* **50**, 2746 (2017).

⁷I. Kassal, J. Yuen-Zhou, and S. Rahimi-Keshari, *Journal of Physical Chemistry Letters* **4**, 362 (2013).

⁸J. Yuen-Zhou, J. J. Krich, M. Mohseni, and A. Aspuru-Guzik, *Proceedings of the National Academy of Sciences of the United States of America* **108**, 17615 (2011).

⁹G. C. Knee, M. Marcus, L. D. Smith, and A. Datta, *Physical Review A* **98**, 052328 (2018).

¹⁰M. Marcus, G. C. Knee, and A. Datta, *Faraday Discussions* **221**, 110 (2020).

¹¹D. J. Tannor, *Introduction to quantum mechanics: a time-dependent perspective* (University Science, Sausalito, 2007).

¹²J. Yuen-Zhou, J. J. Krich, I. Kassal, A. S. Johnson, and A. Aspuru-Guzik, *Ultrafast spectroscopy: quantum information and wavepackets* (IOP Publishing Ltd., Bristol, 2014).

¹³The RWA assumes that $\omega + \omega_0 \gg |\omega - \omega_0|$, which evidently breaks down as $\omega \rightarrow 0$.

¹⁴P. F. Tekavec, G. A. Lott, and A. H. Marcus, *Journal of Chemical Physics* **127**, 214307 (2007).

¹⁵P. Hamm and M. T. Zanni, *Concepts and methods of 2d infrared spectroscopy* (Cambridge University Press, Cambridge, 2011).

¹⁶S. Al-Assam, S. R. Clark, and D. Jaksch, *Journal of Statistical Mechanics* , 093102 (2017).

¹⁷R. Kubo, *Advances in Chemical Physics* **15**, 101 (1969).

¹⁸W. Barford, *Electronic and optical properties of conjugated polymers*, 2nd ed. (Oxford University Press, Oxford, 2013).

¹⁹For a uniform chain $c_{nj} = (2/(N+1))^{1/2} \sin(\pi nj/(N+1))$ and $E_j = 2J \cos(\pi j/(N+1))$.

²⁰W. Barford and M. Marcus, *Journal of Chemical Physics* **145**, 124111 (2016).